Applied Clay Science 47 (2010) 257–262

Contents lists available at ScienceDirect

Applied Clay Science

journal homepage: www.elsevier.com/locate/clay

Synthesis and characterization of bentonite/iron nanoparticles and their application as adsorbent of cobalt ions

T. Shahwan [a,b,*], Ç. Üzüm [a], A.E. Eroğlu [a], I. Lieberwirth [c]

[a] Department of Chemistry, Izmir Institute of Technology, Urla 35430, Izmir, Turkey
[b] Department of Chemistry, Birzeit University, Ramallah, Palestine
[c] Max Planck Institute for Polymer Research, Mainz, Germany

ARTICLE INFO

Article history:
Received 22 December 2008
Received in revised form 27 October 2009
Accepted 28 October 2009
Available online 5 November 2009

Keywords:
Co^{2+}
Iron nanoparticles
Bentonite
Adsorption

ABSTRACT

This study reports the synthesis and characterization of iron nanoparticles in the presence of K10 bentonite. Introducing K10 during synthesis of iron nanoparticles resulted in a partial decrease in the aggregation of the nanoparticles. The dispersed nanoparticles showed a typical core–shell structure and were predominantly within the 10–60 nm size range. The composite adsorbent was tested for the removal of Co^{2+} ions in aqueous solution at various contact times, concentrations, pH, and repetitive loadings. The rate of adsorption was evaluated using first and second order rate equations. The adsorption was described by the Freundlich model. The adsorbent showed effective removal after re-use and the adsorption increased with increasing initial pH.

1. Introduction

Powder and granular forms of iron have been applied as reactive materials in permeable reactive barriers (PRB) for the removal of different pollutants (Blowes et al., 2000). Application of iron nanoparticles should improve the remediation ability of the material by increasing the surface to volume ratios. This technology is expected to provide cost-effective solutions to some of the most challenging environmental cleanup problems and offer enormous flexibility for *in situ* and *ex situ* applications (Zhang, 2003). Although iron nanoparticles have been reported to demonstrate excellent removal capabilities towards various organic and inorganic aqueous pollutants (Ponder et al., 2000; Kanel et al., 2006; Li and Zhang, 2007; Çelebi et al., 2007; Üzüm et al., 2008; Karabelli et al., 2008; Zhang et al., 2006; Varanasi et al., 2007; Liu et al., 2005), adequate delivery and transport models of the material in soil and groundwater bodies is seen as one of the difficulties associated with the application of this technology for *in situ* remediation (Li et al., 2006).

By incorporating iron nanoparticles specifically with minerals that are amenable to geochemical conditions, the delivery of such materials into contaminated sites can be facilitated. By virtue of their wide abundance as well as thermal and structural stability, clay minerals might be suitable materials for hosting iron nanoparticles material. This unique association of iron nanoparticles with clay minerals might be helpful in overcoming problems that relate to the application of the iron nanoparticles technology such as the agglomeration inside water bodies and the relatively high zero point of charge of iron nanoparticles. In spite of the reported advantages, difficulties associated with the direct application of iron nanoparticles for water remediation were discussed (e.g. Zhang, 2003; Huber, 2005; Li et al., 2006). We have reported that the synthesis of iron nanoparticles in the presence of kaolinite decreased the aggregation of the nanoparticles yielding a partial dispersion of them onto the kaolinite surface (Üzüm et al., 2009).

This study reports the synthesis of iron nanoparticles in the presence of K10 bentonite that is composed of montmorillonite, illite, and quartz. The resulting adsorbent was used for the adsorption of Co^{2+} ions from aqueous solution. The adsorbent was characterized using transmission electron microscopy (HR-TEM), scanning electron microscopy (SEM), x-ray diffraction (XRD), electrokinetic mobility measurements, and the BET-N_2 technique. Flame-atomic absorption spectroscopy (FAAS) was used to determine the Co concentration in aqueous solutions.

2. Experimental

2.1. Preparation of the bentonite/iron nanoparticles

In this study $FeCl_2 \cdot 4H_2O$ (ReagentPlus 99%, Sigma-Aldrich 22029-9), $NaBH_4$ (powder 98%, Aldrich 4511-2), bentonite K10 (Aldrich 28152), absolute ethanol (Riedel-de Haën 32221), and $CoCl_2 \cdot 6H_2O$ (Riedel-de Haën 31277) were used without further purification.

The bentonite/iron nanoparticles were prepared by borohydride reduction at a Fe:bentonite mass ratio of 1:5 (Üzüm et al., 2009). 1.07 g $FeCl_2 \cdot 4H_2O$ (corresponding to 0.30 g Fe) was dissolved in a

* Corresponding author. Department of Chemistry, Birzeit University, Ramallah, Palestine. Fax: +970 02 2982084, +90 232 750 7509.
E-mail addresses: tshahwan@birzeit.edu, talalshahwan@iyte.edu.tr (T. Shahwan).

0169-1317/$ – see front matter © 2009 Elsevier B.V. All rights reserved.
doi:10.1016/j.clay.2009.10.019

4:1 (v/v) ethanol/water mixture (24.0 mL ethanol + 6.0 mL deionized water), then 1.50 g of the bentonite was added to this solution and the mixture was left in an ultrasonic shaker for 30 min. Meanwhile, a sodium borohydride solution was prepared by dissolving 0.61 g $NaBH_4$ in 100.0 mL of deionized water. The borohydride solution was added drop-wise to the aqueous bentonite/Fe^{2+} dispersion. After completing addition of the borohydride solution, the dispersion was stirred for an additional 10 min. The reduction of iron ions by borohydride ions is represented by the reaction:

$$>Fe^{2+}(\text{and } Fe^{2+}_{(aq)}) + 2BH^{-}_{4(aq)} + 6H_2O_{(l)} \rightarrow >Fe^{0}_{(s)} + Fe^{0}_{(s)} + 2B(OH)_{3(aq)} + 7H_{2(g)}\uparrow.$$

$>Fe^{2+}$ denotes iron ions attached to the bentonite surface, Fe^{2+} designates aqueous iron ions, $>Fe^{0}_{(s)}$ refers to iron nanoparticles on the bentonite surface, and $Fe^{0}_{(s)}$ stands for unadsorbed iron nanoparticles. The solid material was separated from the liquid phase by vacuum filtration. The solid particles were washed at least three times with 25 mL portions of absolute ethanol, and then were dried overnight at 50 °C.

2.2. Adsorption experiments

Co^{2+} solutions were prepared by dissolving 1.010 g of $CoCl_2 \cdot 6H_2O$ in 250.0 mL of Millipore deionized water (18 MΩ) to yield a 1000.0 mg/L stock. The adsorption experiments were carried out at room temperature (27 ± 3 °C) using 50.0 mL falcon tubes. A Yellowline OS 5 Basic orbital shaker, operating at 350 rpm was used for mixing. After the desired shaking period, the tubes were centrifuged at 6000 rpm. The Co concentration in the supernatant solutions was determined by FAAS.

To determine the effect of contact time, separate 0.050 g weighings of the adsorbent were added to individual 40.0 mL portions of 100.0 mg/L Co^{2+} solutions and dispersed for 1 min, 5 min, 10 min, 30 min, 1 h, 2 h, 4 h, 8 h, 16 h, and 24 h periods.

The effect of initial Co^{2+} concentration on the extent of adsorption was investigated by placing the 40.0 mL aliquots of Co^{2+} solutions (1.0 mg/L, 5.0 mg/L, 10.0 mg/L, 50.0 mg/L, 100.0 mg/L, 250.0 mg/L and 500.0 mg/L) in contact with their respective 0.050 g bentonite/iron nanoparticles sample portions. The dispersions were shaken for 24 h. For the sake of comparison, parallel experiments were also performed using pure iron nanoparticles and pure bentonite samples under the same conditions.

To test the effect of adsorbent concentration on the extent of Co^{2+} adsorption, 0.050 g of bentonite/iron nanoparticles was added to Co^{2+} solution having volumes of 10.0, 20.0, 30.0 and 40.0 mL and mixed for 24 h. This corresponded to *V*/*m* ratios of 200, 400, 600, and 800 (mL/g), respectively. The initial Co^{2+} concentrations were 50.0 mg/L and 500.0 mg/L.

The effect of pH was studied by adjusting the initial pH values to 4.0, 6.0, 8.0 and 10.0 using 0.10 M and/or 1.0 M HNO_3 or NaOH. For each experiment, separate 0.050 g samples of bentonite/iron nanoparticles were placed into their respective solutions of 40.0 mL of 100.0 mg/L Co^{2+}. The pHs of the solutions were measured at the beginning and at the end of the shaking process.

A series of repetitive experiments were performed to study the reusability of the adsorbent. In each experiment, a 0.20 g sample of bentonite/iron nanoparticles was added to either 10.0 mL of 5.0 mg/L or 100.0 mg/L aliquots of Co^{2+} solution. After a shaking period of 45 min, the mixtures were centrifuged and the supernatant solutions were transferred into clean tubes. A 10.0 mL portion of the fresh Co^{2+} solution possessing the same initial concentration was added onto the solid sample that remained in the tube. After a further shaking period of 45 min, the liquid phase was separated again and kept for the analysis. In this way, the adsorbent was exposed to eight successive doses of 10.0 mL solutions.

2.3. Characterization techniques

The surface area of the bentonite/iron nanoparticles samples was determined by the BET-N_2 method using a Micromeritics Gemini 5 type instrument. The samples were degassed for 3 h at 353 K. To identify the point of zero charge (pzc) of the bentonite/iron nanoparticles samples, the electrophoretic mobility was measured for a series of dispersions at a concentration of 0.1 g/L using a Zeta-Meter 3.0 instrument.

The filtrate was analyzed for the Co content via flame AAS using a Thermo Elemental SOLAAR M6 Series atomic absorption spectrometer with an air–acetylene flame. Accuracy was checked through spike tests on the supernatant solutions and it was verified that the aqueous calibration plot could successfully be used in the calculation of the sorption results.

The XRD analysis was done with a Philips X'Pert Pro instrument (Cu K_α radiation). SEM/EDX analysis was performed using a Philips XL-30S FEG type instrument. TEM characterization of the adsorbent was performed using a Tecnai F20 instrument from FEI, operated at 200 kV acceleration voltage. Prior to analysis, the sample was dispersed in ethanol using an ultrasonic bath. Subsequently, a drop of the dispersion was applied to a holey carbon TEM support grid and excess solution was blotted off with filter paper.

3. Results and discussion

3.1. Characterization of the bentonite/iron nanoparticles

The bentonite/iron nanoparticles predominantly had an opaque-black appearance. A typical XRD pattern of bentonite prior to the reaction is given in Fig. 1. The inset in the figure shows the composite material. The presence of metallic iron is indicated by the major reflection at 2θ of 44.7°. In addition, reflections of maghemite (γ-Fe_2O_3), or magnetite (Fe_3O_4), and lepidocrocite (γ-FeOOH) were observed. The strong reflection of γ-Fe_2O_3 and Fe_3O_4 superimposed.

While some of the iron nanoparticles were dispersed on the bentonite particles, another part exhibited a characteristic chain-like morphology (Fig. 2). HR-TEM images (Fig. 3) showed both forms and demonstrated also the core–shell structure of iron nanoparticles. The particle diameter ranged within 10–60 nm, with the shell thickness of 3–4 nm. The absence of the lattice fringes in the HR-TEM images indicated that the shell was amorphous. The thickness of the shell in the dispersed nanoparticles and chain-like morphology were similar. The shell in the nanoparticles is known to play a dual role. It preserves the iron core against fast oxidation (e.g. Li and Zhang, 2007; Karabelli

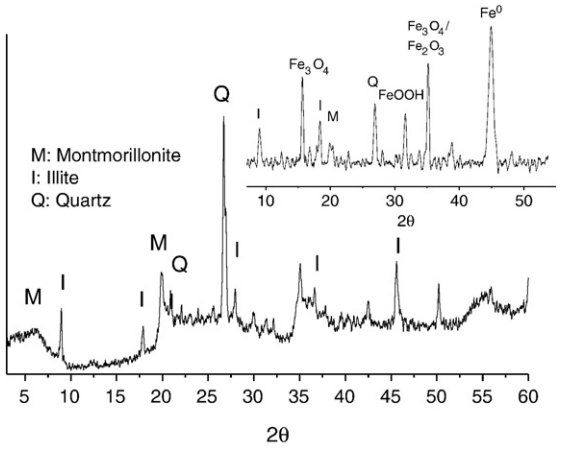

Fig. 1. XRD diagram of K10 bentonite. The inset shows the diagram of the bentonite/iron nanoparticles.

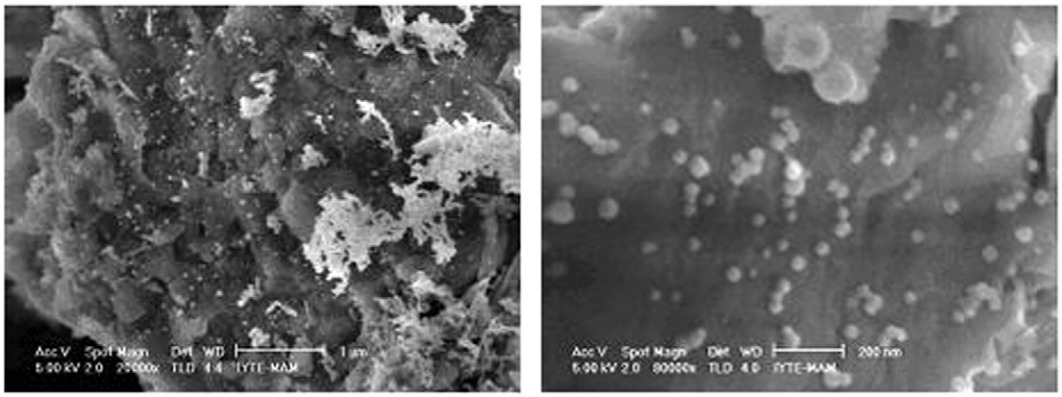

Fig. 2. SEM images of the bentonite/iron nanoparticles adsorbent at two different magnifications.

et al., 2008; Li et al., 2006). The presence of FeOOH groups at the external surface has an important function in the adsorption mechanism (Li and Zhang, 2007). HR-TEM images for bentonite/iron nanoparticles samples stored under atmospheric conditions showed that the nanoparticles seemed to retain their dispersion on the bentonite particles over time. Fig. 3d shows a sample aged for six months at atmospheric conditions. The shell thickness after the given period was around 5 nm, indicating a slow advancement in oxidation.

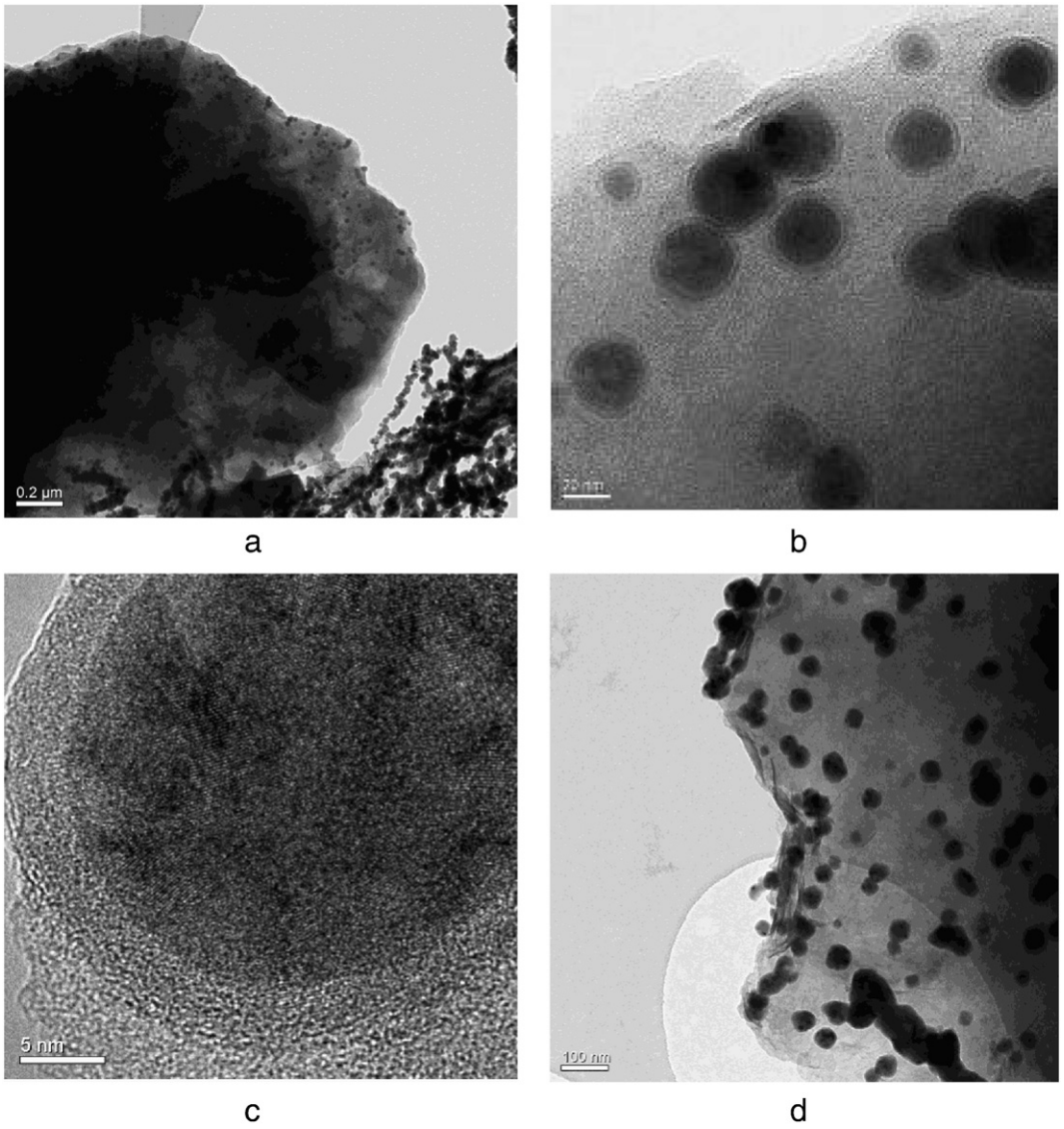

Fig. 3. HR-TEM images of: a) iron nanoparticles both in chain-like morphology and in dispersed form on the bentonite surface, b) iron nanoparticles on bentonite surface, c) the core–shell structure of iron nanoparticles, and d) iron nanoparticles on bentonite surface six months after preparation.

The specific BET surface area of the adsorbent was 66.5 m^2/g, in comparison to 57.3 m^2/g for K10. The variation of electrophoretic mobility of the bentonite/iron nanoparticles adsorbent as a function of pH (Fig. 4) indicated a pzc at pH = 2.8. This is due to the presence of the bentonite in 5:1 ratio in the composite adsorbent. Fe nanoparticles possessed a pzc at pH = 8.1–8.2 (Çelebi et al., 2007; Üzüm et al., 2008; Sun et al., 2006).

3.2. Co^{2+} adsorption

3.2.1. Adsorption kinetics

The adsorption of Co^{2+} ions approached equilibrium in about 1 h (Fig. 5). The data were described by the first and second order rate equations for the removal of Co from aqueous solution which might be written as follows:

$$-\frac{dC_t}{dt} = k_1(C_t - C_e) \quad (1)$$

$$-\frac{dC_t}{dt} = k_2(C_t - C_e)^2. \quad (2)$$

Integrating under the boundary conditions $C_t = C_0$ at $t = 0$ and $C_t = C_t$ at $t = t$ yields:

$$\ln\left(\frac{C_t - C_e}{C_0 - C_e}\right) = -k_1 t \quad (3)$$

$$\frac{1}{C_t - C_e} - \frac{1}{C_0 - C_e} = k_2 t. \quad (4)$$

The term $C_0 - C_e$ in both equations is a fixed parameter for a given set of experimental data at a certain initial concentration. Eq. (3) can be easily transformed into the well known Lagergren's equation (pseudo-first order rate equation) if expressed in terms of the adsorbate concentration on the solid phase, q_t, by the mass balance formula:

$$C_0 - C_t = q_t \frac{M}{V} \quad (5)$$

Here M is the mass of the adsorbent and V is the volume of the solution used in adsorption experiments.

Eqs. (3) and (4) were plotted against time of the presaturation interval, up to 60 min of contact time (inset in Fig. 5). The linear regression analysis showed that the data correlated better with the second order kinetics (Eq. (4)). The rate constants and linear correlation coefficients were 0.0353 min^{-1} and 0.9218 for the first order kinetics, and 0.0172 L mg^{-1} min^{-1} and 0.9748 for the second order kinetics.

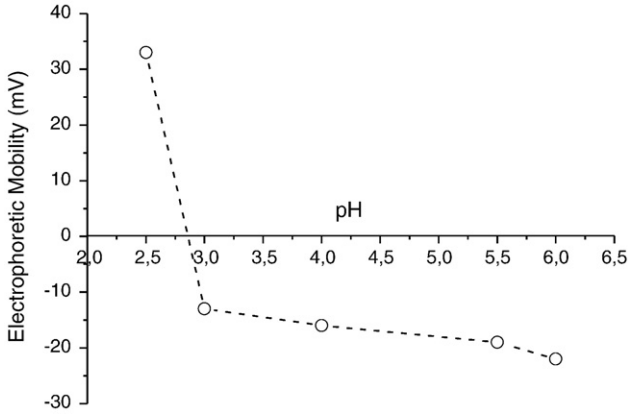

Fig. 4. Electrophoretic mobility data of bentonite/iron nanoparticles.

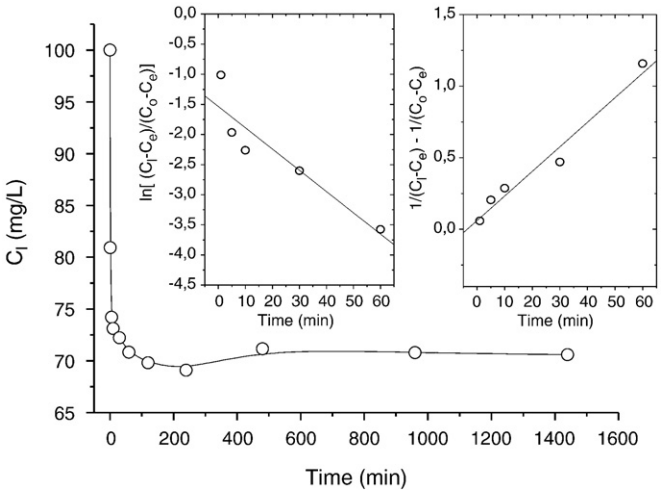

Fig. 5. Concentration of Co^{2+} ions in solution (mg/L) as a function of time. The insets show the linear fits obtained for the first 5 data sets using Eqs. (3) and (4).

The data were also tested using Ho's equation (pseudo second order equation) over the entire time range as recommended by the author (Ho, 2006):

$$\frac{t}{q_t} = \frac{1}{k_2 q_e^2} + \frac{1}{q_e} t \quad (6)$$

In spite of the almost perfect correlation with the entire range of data, the intercept was negative, a physically impossible situation. However, when the data corresponding to only the presaturation interval were used, the problem was fixed and the linear fit yielded a rate constant of 0.04727 g mg^{-1} min^{-1} with a linear correlation coefficient of 0.9998.

3.2.2. Effect of initial Co^{2+} concentration

Adsorption of Co^{2+} at different initial concentrations is shown in Fig. 6. As expected, the adsorption capacity of the bentonite/iron nanoparticles composite was smaller than that of pure iron nanoparticles but was significantly enhanced in comparison to the bentonite K10.

The adsorption isotherm was of L-type without reaching a saturation plateau (Fig. 7). This class of isotherms indicates that the ratio between the concentrations of the adsorptive remaining in solution and that adsorbed on the solid increases with increasing

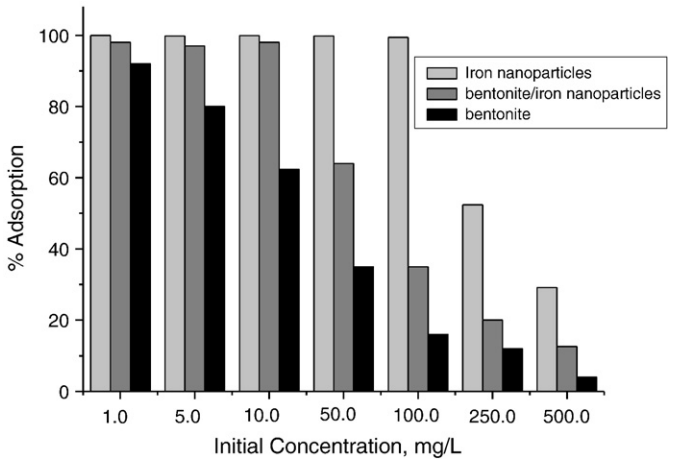

Fig. 6. Adsorption data of Co^{2+} ions on iron nanoparticles, bentonite/iron nanoparticles, and bentonite with respect to initial cation concentration.

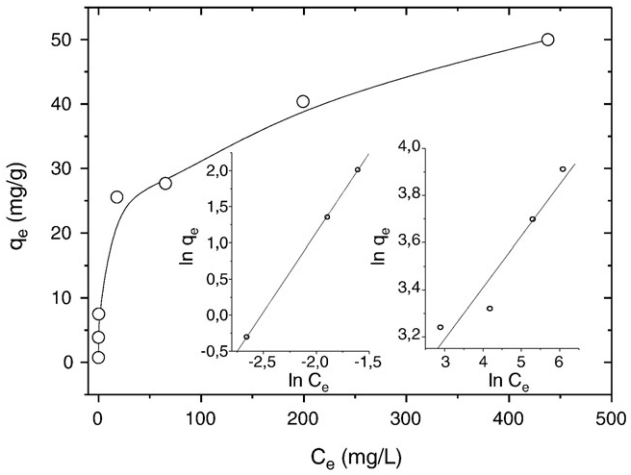

Fig. 7. Equilibrium Co^{2+} concentration on the solid adsorbent as a function of its liquid concentration. The insets show Freundlich isotherm plots at two different ranges of concentration.

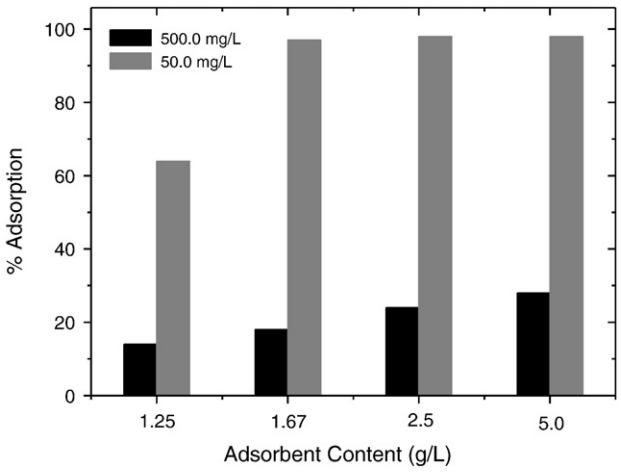

Fig. 8. Variation of Co^{2+} adsorption with respect to adsorbent content at two initial concentrations.

solute concentration, providing a concave curve as a result of progressive saturation of the solid (Limousin et al., 2007).

The adsorption data were fitted to the Freundlich equation,

$$q_e = kC_e^N \quad (7)$$

The total isotherm could not be fitted by the Freundlich equation but two linear sections were obtained in the linearized representation (inserts in Fig. 7, Table 1). The values of the constants were strongly dependent on the concentration range, with much higher adsorption affinity observed at the lower range of concentrations.

The results given in this section were obtained at the adsorbent concentration of 1.25 g/L. In this case, the adsorption of Co^{2+} was almost quantitative up to the initial concentration of 50.0 mg/L. Fig. 8 indicates that nearly complete removal of Co^{2+} ions from 50.0 mg/L solutions was possible using less than 2 g/L adsorbent content, indicating the effectiveness of the adsorbent.

3.2.3. Reusability of the bentonite/iron nanoparticles

The adsorbent effectively removed Co^{2+} ions from aqueous solution even after 8 successive uses (Fig. 9). When the Co^{2+} concentration was increased to 100.0 mg/L, more than 90% of Co^{2+} was adsorbed after three uses. Taking into account that the concentrations of Co^{2+} ions in underground water and even in industrial wastewaters are usually lower than 100.0 mg/L, multiple usage of the material at low concentrations seems to be possible.

3.2.4. Effect of pH

As previously reported, the fixation of Co^{2+} ions takes place by oxyhydroxyl groups of iron nanoparticles rather than through a redox reaction in spite of the fact that Co is somewhat higher in the electrochemical series than Fe (Üzüm et al., 2008). XPS data of Co adsorbed on iron nanoparticles are given in Fig. 10. We reported this mechanism also for iron nanoparticles on kaolinite (Üzüm et al., 2009). As shown in Table 2, the adsorption of Co^{2+} ions increased with the increasing initial pH of the dispersion. The increase of the adsorbed amounts with pH seems to be steeper than the change of the

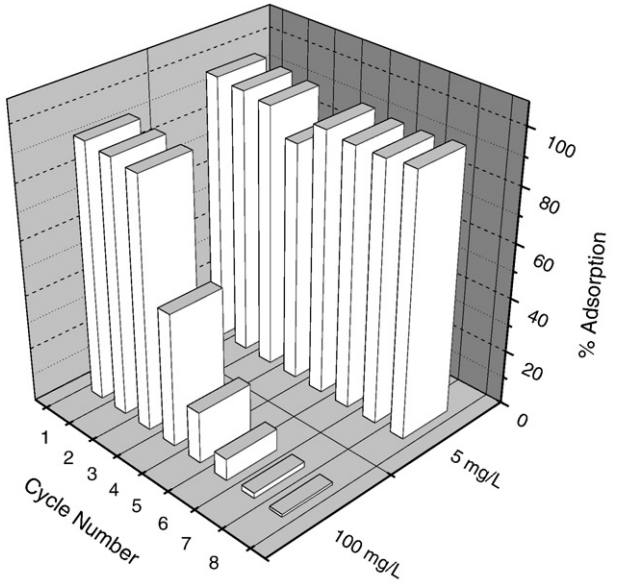

Fig. 9. Adsorption in the reusability experiments at two initial concentrations of Co^{2+} ions.

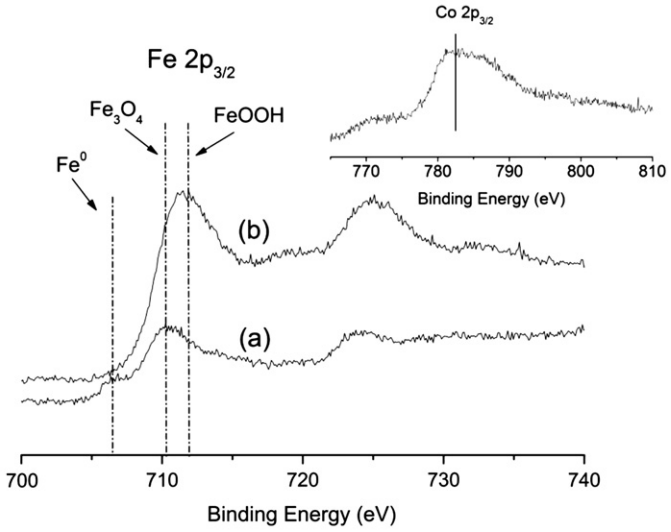

Fig. 10. XPS spectra of: (a) Fe^0 standard, (b) iron nanoparticles. The inset in the figure shows the XPS spectrum of Co^{2+} after fixation at the surface of iron nanoparticles.

Table 1
The values of Freundlich constants obtained at two ranges of Co^{2+} initial concentrations.

Concentration range, mg/L	*k*	*N*	*R*
1.0–10.0	254.4	2.20	0.9999
50.0–500.0	12.6	0.22	0.9591

Table 2
Adsorption of 100 mg/L Co^{2+} ions by bentonite/iron nanoparticles at various initial pH values.

pH	C_e (mg/L)	% Adsorption
4.0	50.7	49
6.0	43.5	57
8.0	28.7	71
10.0	11.6	88

electrophoretic mobility. The relation to the change of the zpc is complicated by the inhomogeneous nature of the composite material when some of the nanoparticles were dispersed on the bentonite surface while another part retained the well known chain-like morphology of iron nanoparticles.

4. Conclusions

Core–shell iron nanoparticles where synthesized in the presence of K10 bentonite. The adsorption of Co^{2+} ions was described by the second order rate equation. Within the studied concentration range, the equilibrium data adequately obeyed the Freundlich isotherm. The adsorbent seems to be appropriate for multiple usages at low Co^{2+} concentration. The amount of adsorbed Co^{2+} ions increased due to deprotonation of oxyhydroxyl groups on the external surface of the core–shell iron nanoparticles. More effort is still required to elaborate on the relationship between the precursor concentrations of Fe^{2+} and the clay mineral at the stage of adsorbent synthesis in order to achieve better dispersion of the nanoparticles on the clay mineral particles.

Acknowledgements

This work was financed by Izmir Institute of Technology (project no. 2006-IYTE-13). The authors thank the Center of Material Research (İYTE-MAM) at İzmir Institute of Technology for the assistance in the SEM and XRD measurements. The authors thank Dr. K. R. Hallam and Dr. T. B. Scott at the Interface Analysis Centre, University of Bristol for their help in XPS analysis. The authors are grateful to Dr. Ritchie Eanes for the proofreading of the manuscript.

References

Blowes, D.W., Ptacek, C.J., Benner, S.G., McRae Che, W.T., Bennett, T.A., Puls, R.W., 2000. Treatment of inorganic contaminants using permeable reactive barriers. J. Contam. Hydrol. 45, 123–137.

Çelebi, O., Üzüm, Ç., Shahwan, T., Erten, H.N., 2007. A radiotracer study of the adsorption behavior of aqueous Ba^{2+} ions on nanoparticles of zero-valent iron. J. Hazard. Mater. 148, 761–767.

Ho, Y.-S., 2006. Review of second-order models for adsorption systems. J. Hazard. Mater. 136, 681–689.

Huber, D.L., 2005. Synthesis, properties, and applications of iron nanoparticles. Small 1, 482–501.

Kanel, S.R., Greneche, J.M., Choi, H., 2006. Arsenic(V) removal from groundwater using nano scale zero-valent iron as a colloidal reactive barrier material. Environ. Sci. Technol. 40, 2045–2050.

Karabelli, D., Uzum, C., Shahwan, T., Eroglu, A.E., Scott, T., Hallam, K.R., Lieberwirth, I., 2008. Batch removal of aqueous Cu^{2+} ions using nanoparticles of zero-valent iron: a study of the capacity and mechanism of uptake. Ind. Eng. Chem. Res. 47, 4758–4764.

Li, X.-q., Zhang, W.-x., 2007. Sequestration of metal cations with zerovalent iron nanoparticles — a study with high resolution x-ray photoelectron spectroscopy (HR-XPS). J. Phys. Chem. C. 111, 6939–6946.

Li, L., Fan, M., Brown, R.C., Leeuwen, J.V., Wang, J., Wang, W., Song, Y., Zhang, P., 2006. Synthesis, properties, and environmental applications of nanoscale iron-based materials: a review. Crit. Rev. Environ. Sci. Technol. 36, 405–431.

Limousin, G., Gaudet, J.-P., Charlet, L., Szenknect, S., Barthès, V., Krimissa, M., 2007. Sorption isotherms: a review on physical bases, modeling and measurement. Appl. Geochem. 22, 249–275.

Liu, Y., Majetich, S.A., Tilton, R.D., Sholl, D.S., Lowry, G.V., 2005. TCE dechlorination rates, pathways, and efficiency of nanoscale iron particles with different properties. Environ. Sci. Technol. 39, 1338–1345.

Ponder, S.M., Darab, J.G., Mallouk, T.E., 2000. Remediation of Cr(VI) and Pb(II) aqueous solutions using nanoscale zero-valent iron. Environ. Sci. Technol. 34, 2564–2569.

Sun, Y., Li, X., Cao, J., Zhang, W., Wang, H.P., 2006. Characterization of zero-valent iron nanoparticles. Adv. Colloid Interface Sci. 120, 47–56.

Üzüm, Ç., Shahwan, T., Eroğlu, A.E., Lieberwirth, I., Scott, T.B., Hallam, K.R., 2008. Application of zero-valent iron nanoparticles for the removal of aqueous Co^{2+} ions under various experimental conditions. Chem. Eng. J. 144, 213–220.

Üzüm, Ç., Shahwan, T., Eroğlu, A.E., Hallam, K.R., Scott, T.B., Lieberwirth, I., 2009. Synthesis and characterization of kaolinite-supported zero-valent iron nanoparticles and their application for the removal of aqueous Cu^{2+} and Co^{2+} ions. Appl. Clay Sci. 43, 172–181.

Varanasi, P., Fullana, A., Sidhu, S., 2007. Remediation of PCB contaminated soils using iron nano-particles. Chemosphere 66, 1031–1038.

Zhang, W.-x., 2003. Nanoscale iron particles for environmental remediation: an overview. J. Nanopart. Res. 5, 323–332.

Zhang, H., Jin, Z.-h., Han, L., Qin, C.-h., 2006. Synthesis of nanoscale zero-valent iron supported on exfoliated graphite for removal of nitrate. T Nonferr. Metal Soc. China 16, s345–s349.